Supplementary material

Too young or too old: evaluating cosmogenic exposure dating based on an analysis of compiled boulder exposure ages

Jakob Heyman[a*], Arjen P. Stroeven[a], Jonathan M. Harbor[b], Marc W. Caffee[c]

[a] *Department of Physical Geography and Quaternary Geology, Stockholm University, 106 91 Stockholm, Sweden*
[b] *Department of Earth and Atmospheric Sciences, Purdue University, West Lafayette, IN 47907-1397, USA*
[c] *Department of Physics, Purdue Rare Isotope Measurement Laboratory, Purdue University, West Lafayette, IN 47907-1397, USA*
[*] *E-mail:* jakob.heyman@natgeo.su.se

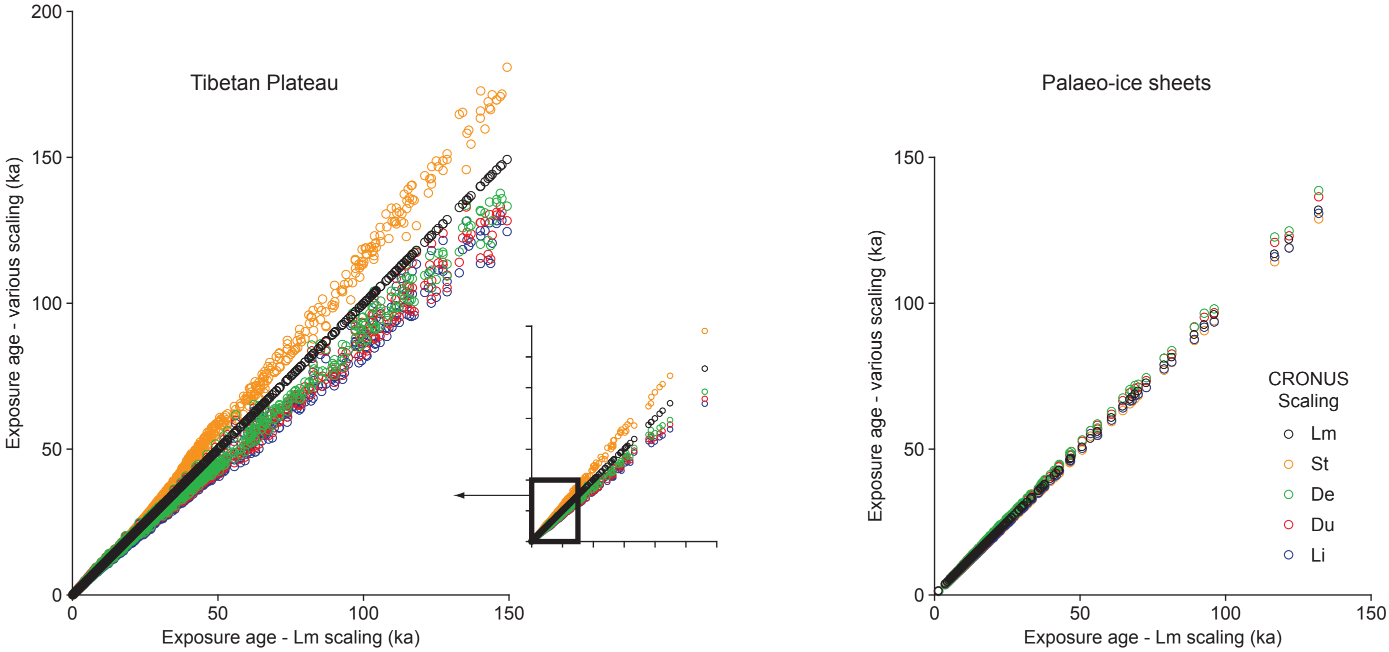

Fig. S1. Exposure age variation between five different CRONUS production rate scaling schemes. Exposure ages from the Tibetan Plateau and the Northern Hemisphere palaeo-ice sheet glacial boulder datasets were calculated using five different scaling schemes in the CRONUS online calculator (Balco et al., 2008) and they are plotted against the equivalent CRONUS Lm exposure ages used in this study. The inset in the left panel shows the full dataset for the Tibetan Plateau. For description of the different scaling schemes, see Balco et al. (2008). The exposure ages of the Tibetan Plateau boulders vary significantly more between the various scaling schemes than the palaeo-ice sheet boulders (reflecting a lack of production rate calibration sites on the Tibetan Plateau). Changing the employed production rate scaling scheme (Lm) to another alters the individual exposure ages of the Tibetan Plateau boulders significantly, in particular the old exposure ages. However, the large-scale pattern of the exposure age dataset does not change dramatically, and our conclusions are valid for all five production rate scaling schemes. For exposure age data, see Supplementary Dataset.

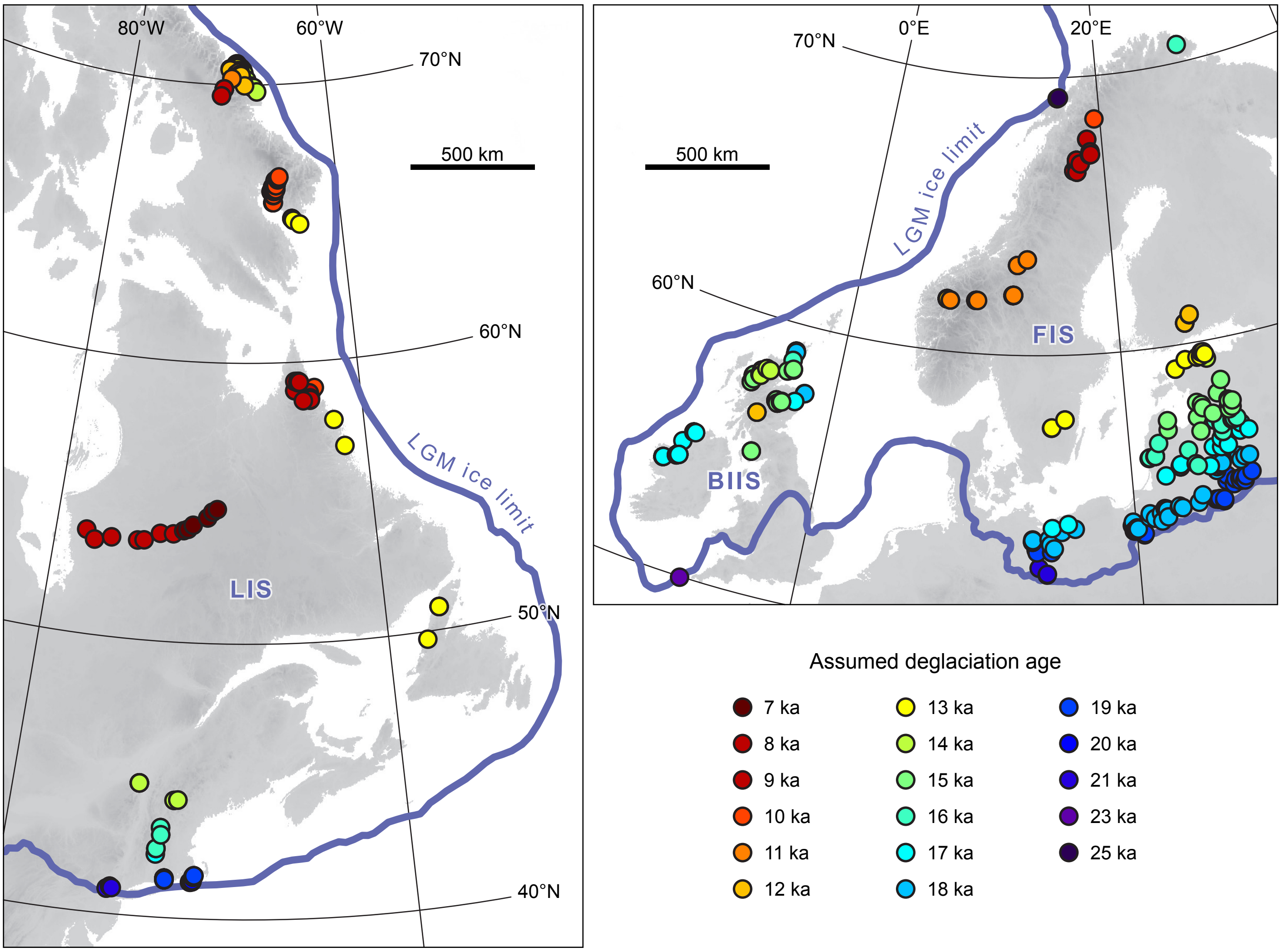

Fig. S2. Assumed deglaciation ages for exposure age inaccuracy quantification of the palaeo-ice sheet dataset. The deglaciation ages for the Laurentide ice sheet (LIS) are based on reconstructions presented by Dyke et al. (2003) and Kleman et al. (2010). The deglaciation ages for the British Irish (BIIS) and Fennoscandian ice sheet (FIS) are based on the reconstruction presented by Gyllencreutz et al. (2007a). For sample-specific assumed deglaciation ages, see Supplementary Dataset.

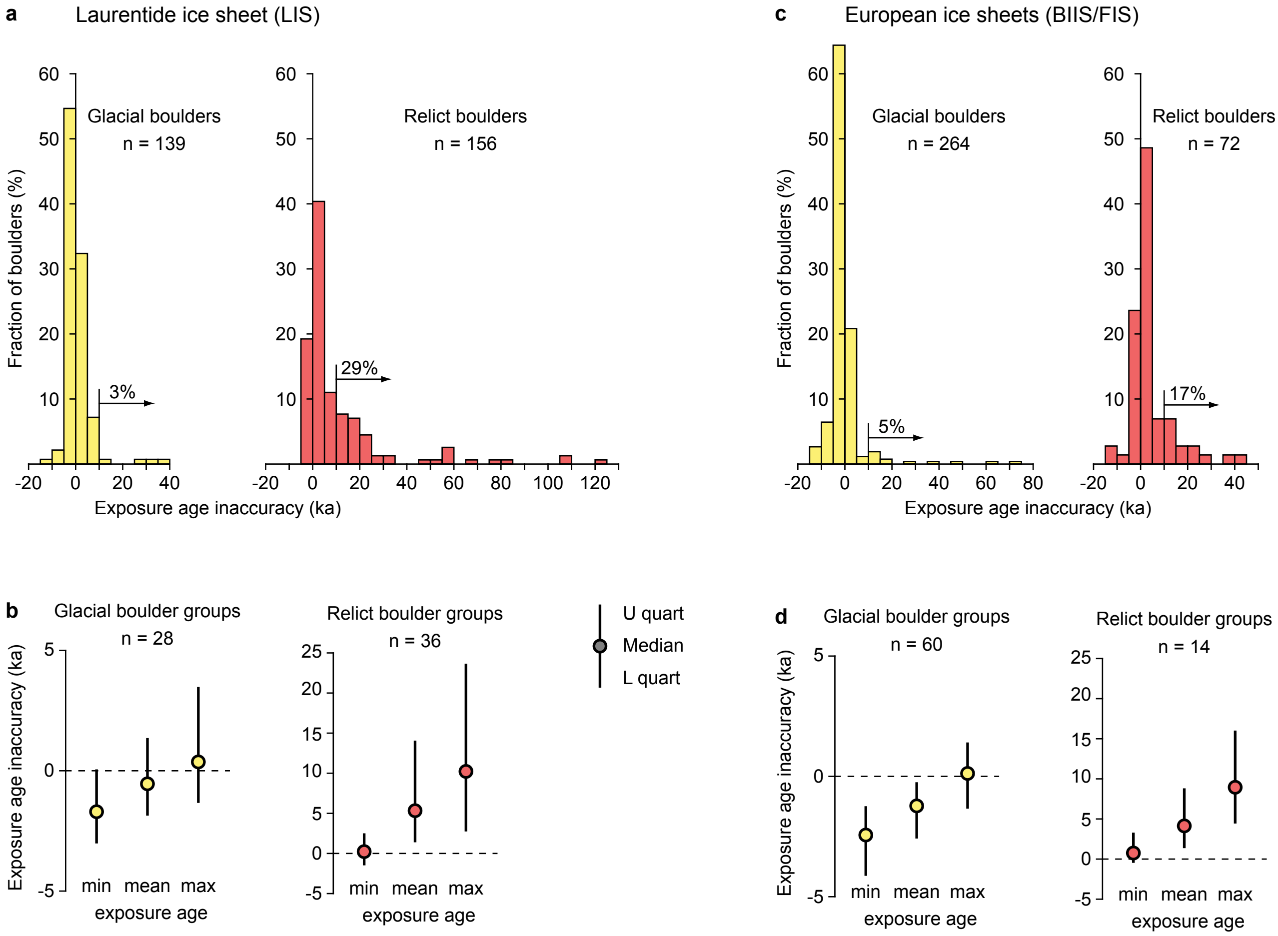

Fig. S3. Palaeo-ice sheet boulder exposure age inaccuracy, defined as ^{10}Be apparent exposure age minus corresponding reconstructed deglaciation age (cf. Fig. S2; Dyke et al., 2003; Gyllencreutz et al., 2007a,b; Kleman et al., 2010), divided between the Laurentide and the European ice sheet areas. (a) Exposure age inaccuracy of individual boulders from the Laurentide palaeo-ice sheet area divided into 5 ka bins (horizontal axis). (b) Exposure age inaccuracy of multiple-boulder group (≥2 boulders per group) minimum, mean, and maximum exposure ages from the Laurentide palaeo-ice sheet area shown as median and interquartile range. (c) Exposure age inaccuracy of individual boulders from the European palaeo-ice sheet area divided into 5 ka bins. (d) Exposure age inaccuracy of multiple-boulder group minimum, mean, and maximum exposure ages from the European palaeo-ice sheet area shown as median and interquartile range. The chronologies of all deglaciation reconstructions (Dyke et al., 2003; Kleman et al., 2010; Gyllencreutz et al., 2007a,b) are based primarily on radiocarbon dates. However, while the European deglaciation age database includes cosmogenic exposure ages the Laurentide deglaciation age database does not include any cosmogenic exposure ages. Hence, the Laurentide deglaciation reconstructions offer more independent deglaciation ages for comparison with the apparent exposure ages. The quantified inaccuracy of the Laurentide and European palaeo-ice sheet boulder exposure age datasets are largely similar, with low percentages of boulders in glacially modified areas having exposure ages more than 10 ka older than the corresponding deglaciation reconstruction ages (3% and 5%, respectively).

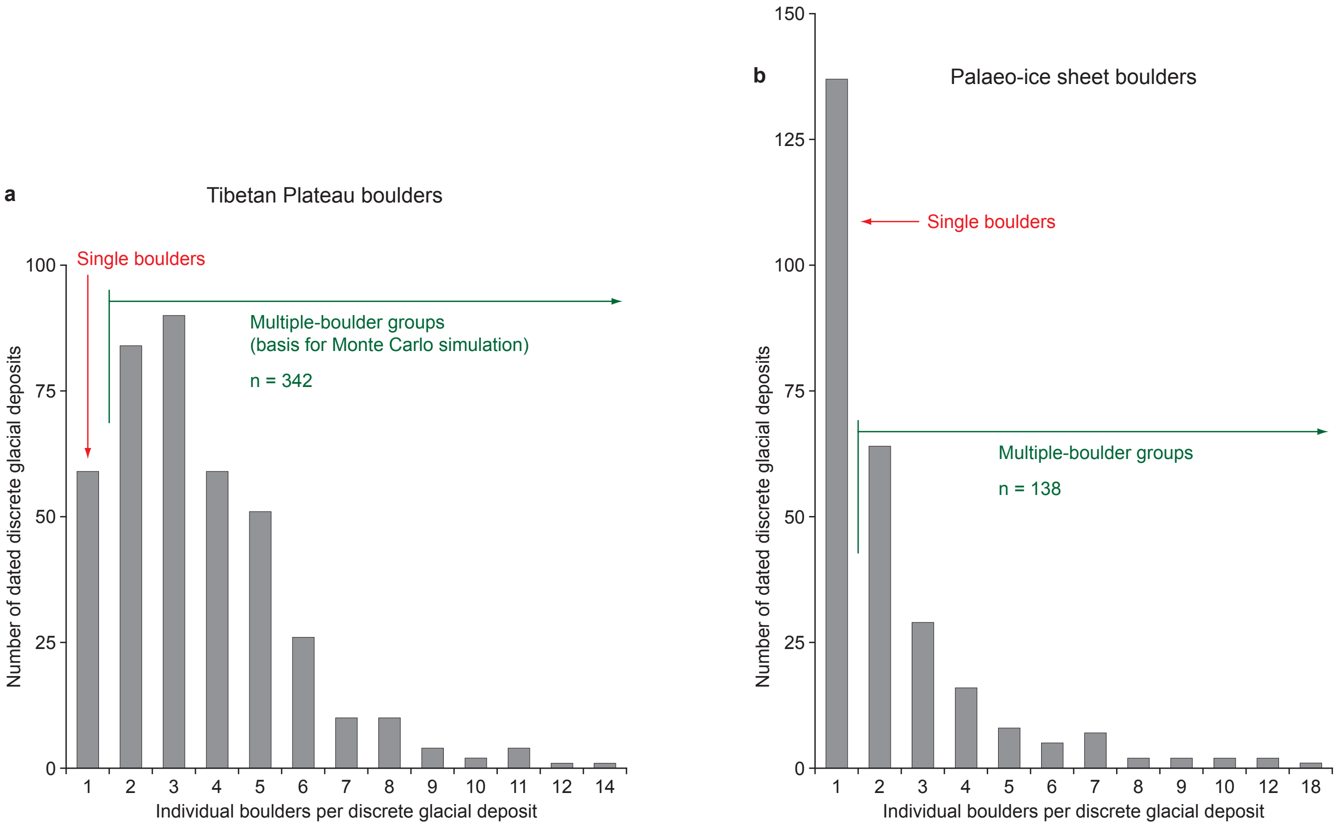

Fig. S4. Number of dated discrete glacial deposits (vertical axis) where 1 to 18 individual boulders (horizontal axis) were sampled for each discrete glacial deposit. (a) Boulders from the Tibetan Plateau. (b) Boulders from the Palaeo-ice sheet areas. The ages from a large majority of all cosmogenic exposure dated discrete glacial deposits are based on 1-5 dated boulders. For data and grouping of boulders, see Supplementary Dataset.

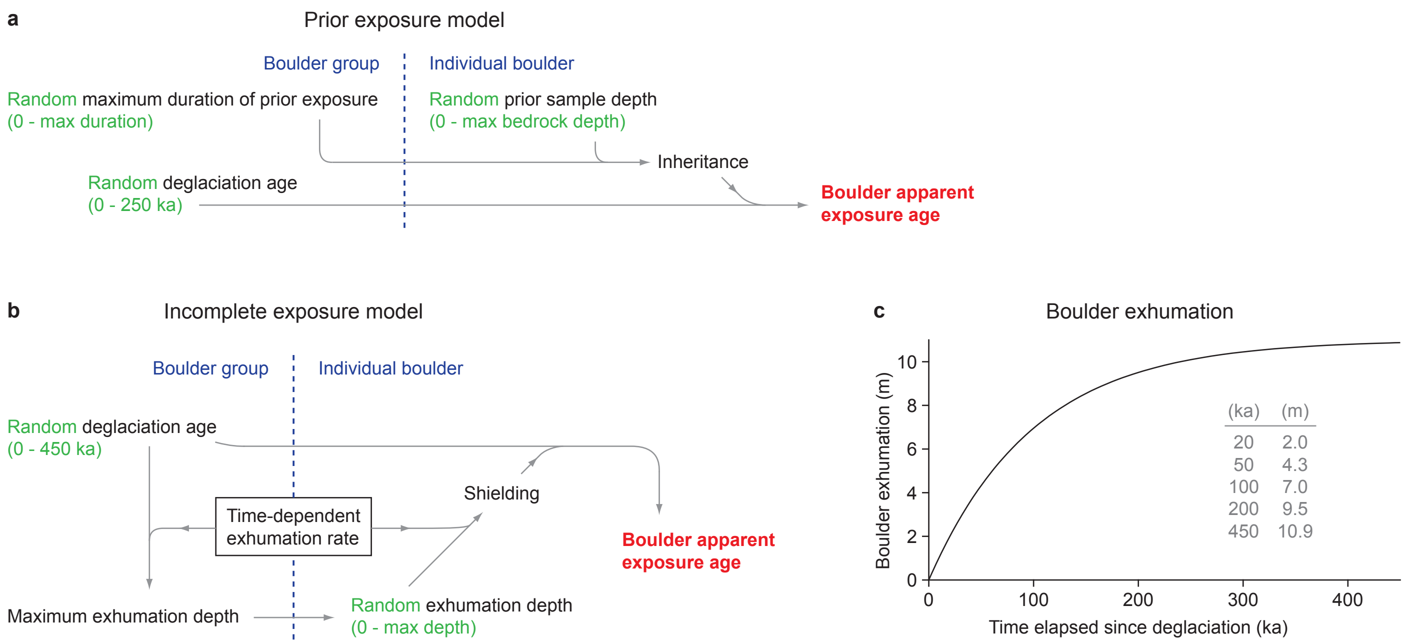

Fig. S5. Monte Carlo simulation of boulder apparent exposure ages of Tibetan Plateau multiple-boulder glacial deposits. (a) Flow chart of the prior exposure simulation. (b) Flow chart of the incomplete exposure simulation. (c) Time-dependent boulder exhumation curve adopted for all boulders in the incomplete exposure simulation.

Exposure age simulations

In the Monte Carlo simulations of prior exposure and incomplete exposure, the apparent exposure age is calculated for multiples of all Tibetan Plateau boulder groups (Fig. S4a). Randomised factors regarding the geological history of the boulders yield various ^{10}Be concentrations and apparent exposure ages.

Production of ^{10}Be occurs by high-energy spallation and muon interaction (Granger and Smith, 2000; Gosse and Phillips, 2001) with a production rate P_d (atoms g^{-1} yr^{-1}) at the depth d (cm) below the surface:

$$P_d = f_s P_0 e^{-\rho d/\Lambda} + f_m P_0 (m_1 e^{-\rho d/L1} + m_2 e^{-\rho d/L2} + m_3 e^{-\rho d/L3}) \quad (1)$$

where the first term represents the production rate due to spallation (Lal, 1991) and the second term represents the production rate due to muon interaction (Granger and Smith, 2000). The coefficients f_s and f_m are the spallogenic and muogenic fractions (dimensionless), respectively, of the surface production rate P_0 (d = 0), with f_s = 0.988 and f_m = 0.012 based on average surface production rates of the measured Tibetan Plateau boulders (CRONUS muon and St spallation production rates; see Supplementary Dataset). The coefficient ρ is the mean density (g cm^{-3}) of the shielding material, here 2.7 g cm^{-3} for bedrock, and Λ is the attenuation length (g cm^{-2}) for spallogenic production, here 160 g cm^{-2} (cf. Gosse and Phillips, 2001; Balco et al., 2008). The coefficients m_1 = 0.76, m_2 = 0.11, and m_3 = 0.13 are dimensionless coefficients based on the approximation of sub-surface muogenic production presented by Granger and Smith (2000) with scaling of the sea level high latitude factors using an atmospheric depth difference of 400 g cm^{-2} (corresponding to altitudes of c. 4000 m a.s.l.) and the attenuation lengths L1 = 738.6 g cm^{-2}, L2 = 2688 g cm^{-2}, and L3 = 4360 g cm^{-2} (Granger and Smith, 2000).

The apparent exposure age A (yr) of a sample, assuming no shielding from cosmic rays, is based on Lal (1991):

$$A = \ln (1 - N \lambda / P_0) / -\lambda \quad (2)$$

where N is the sample ^{10}Be concentration (atoms g^{-1}), λ is the ^{10}Be decay constant (yr^{-1}) with a value of 4.997 x 10^{-7} (Chmeleff et al., 2010; Korschinek et al., 2010), and P_0 is the surface production rate (atoms g^{-1} yr^{-1}).

Prior exposure model

In the prior exposure model, each boulder group is assigned a random duration of prior exposure T_{pri} (yr) between zero and a maximum value, and a random deglaciation age T_{degl} (yr) between 0 and 250 ka. Each individual sample is assigned a random depth beneath the bedrock surface d_{pri} (cm) between zero and a maximum depth.

The inherited ^{10}Be concentration N_{inh} (atoms g^{-1}) at the time of glacial erosion and deposition is based on Lal (1991):

$$N_{inh} = P_d / \lambda (1 - e^{-\lambda T}) \quad (3)$$

where P_d is given by the depth d_{pri} and Eq. (1), and T is given by T_{pri}.

The inherited ^{10}Be concentration is converted to an inherited apparent exposure age A_{inh} (yr) at the time of glacial erosion and deposition based on Eq. (2) with N based on Eq. (3). Because the ^{10}Be concentration N_{inh} is a product of the surface production rate P_0 (Eq. 1 and 3), the value of P_0 does not influence the acquired apparent exposure age A_{inh}. Thus, the apparent exposure age acquired due to prior exposure varies only with the random duration of prior exposure and the random sample depth beneath the surface.

The apparent exposure age of the sampled boulder T_A (yr) is calculated by summarising the inherited apparent exposure age and the deglaciation age:

$$T_A = A_{inh} + T_{degl} \quad (4)$$

Incomplete exposure model

In the incomplete exposure model all boulders are shielded by and exhumed from till with a specific time-dependent exponential exhumation rate dx/dt (cm yr^{-1}):

$$dx/dt = ae^{-bt} \quad (5)$$

where t is time elapsed since deglaciation (yr) and with the coefficients a = 1.1 x 10^{-2} (cm yr^{-1}) and b = 10^{-5} (yr^{-1}). The values of a and b were chosen to produce exposure age patterns similar to the measured exposure age pattern of the Tibetan Plateau dataset and they yield a maximum of 10.9 m of overburden removal and boulder exhumation after 450 ka (Fig. S5c). Each boulder group is assigned a random deglaciation age T_{degl} (yr) between 0 and 450 ka and each individual boulder has been exhumed/shielded over an exhumation duration T_{exh} (yr) based on a randomized boulder depth at deglaciation d_{degl} (cm; constrained by T_{degl}) and Eq. (5).

Production of ^{10}Be occurs by high-energy spallation and muon interaction (Granger and Smith, 2000; Gosse and Phillips, 2001) with a production rate P_d (atoms g^{-1} yr^{-1}) given by Eq. (1) with the mean density ρ = 2.0 g cm^{-3} for till. The coefficients for spallogenic and muogenic production are the same as in the prior exposure model: f_s = 0.988, f_m = 0.012, Λ = 160 g cm^{-2}, m_1 = 0.76, m_2 = 0.11, m_3 = 0.13, L1 = 738.6 g cm^{-2}, L2 = 2688 g cm^{-2}, and L3 = 4360 g cm^{-2}.

The ^{10}Be concentration in a sample at the time of reaching the surface N_{exh} (atoms g^{-1}) is calculated by summarising the ^{10}Be production and decay for the exhumation duration using time steps Δt:

$$N_{exh} = \sum_{i=1}^{n} P_d \Delta t - N_{i-1} (1 - e^{-\lambda\Delta t}) \quad (6)$$

where Δt is 50 yr, production rate P_d is given by Eq. (1) and with the time-dependent depth d derived from d_{degl} and Eq. (5). The last term of Eq. (6) represents ^{10}Be decay.

The ^{10}Be concentration in a sample at the time of reaching the surface is converted to an apparent exposure age A_{exh} (yr) based on Eq. (2) with N based on Eq. (6). Because the ^{10}Be concentration N_{exh} is a product of the surface production rate P_0 (Eq. 1 and 6), the value of P_0 does not influence the acquired apparent exposure age A_{exh}. Thus, the apparent exposure age acquired during boulder exhumation varies only with the random boulder depth at deglaciation.

The apparent exposure age of the sampled boulder T_A (yr) is calculated by summarising the time elapsed since exhumation and the sub-surface apparent exposure age:

$$T_A = T_{degl} - T_{exh} + A_{exh} \quad (7)$$

Prior/incomplete exposure model

In the combined prior and incomplete exposure model the ^{10}Be concentration in a boulder when it becomes exhumed N_{ie} (atoms g^{-1}) is calculated by summarising the prior exposure and the post-depositional exhumation components:

$$N_{ie} = N_{inh}\, e^{-\lambda T} + N_{exh} \quad (8)$$

where N_{inh} is given by Eq. (3) and subject to decay during the duration T given by the exhumation duration T_{exh}, and N_{exh} is given by Eq. (6).

The ^{10}Be concentration in a sample at the time of reaching the surface is converted to an apparent exposure age A_{ie} (yr) based on Eq. (2) with N based on Eq. (8).

The apparent exposure age of the sampled boulder T_A (yr) is calculated by summarising the inheritance/exhumation component and the time elapsed since exhumation:

$$T_A = A_{ie} + T_{degl} - T_{exh} \quad (9)$$

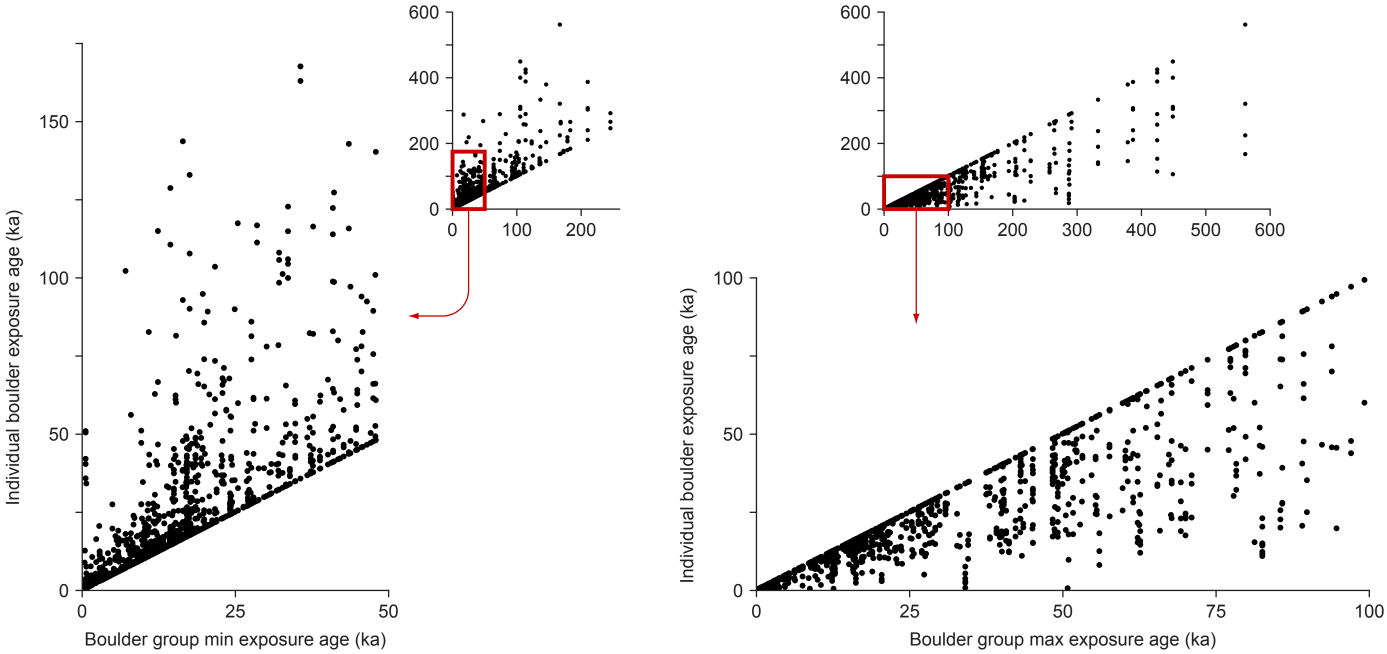

Fig. S6. Measured Tibetan Plateau exposure ages (vertical axis) from multiple-boulder group (≥2 boulders per group) shown against group minimum and maximum exposure age (horizontal axis). A majority of the measured exposure ages fall towards the younger part of the exposure age envelope (cf. Owen et al., 2008).

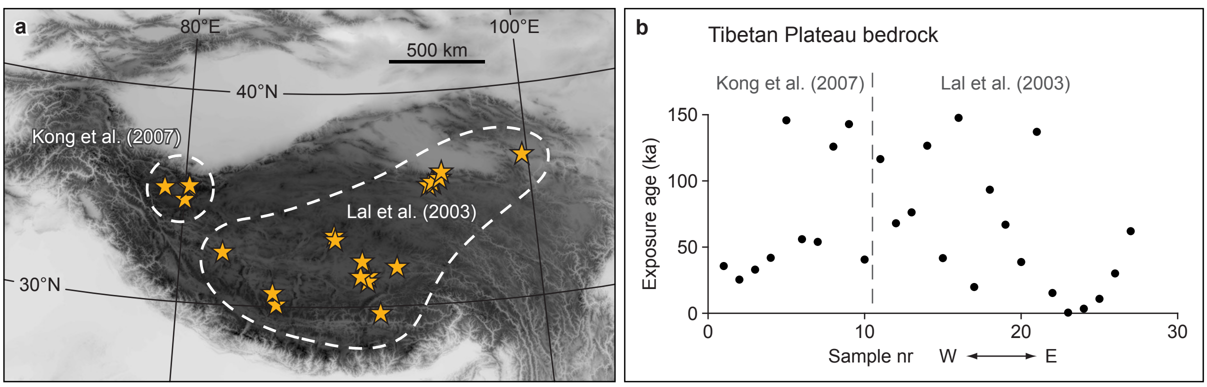

Fig. S7. Tibetan Plateau bedrock surface exposure ages. (a) Location of the bedrock surfaces. (b) Bedrock surface apparent exposure ages (Lal et al., 2003; Kong et al., 2007). The bedrock surfaces have been collected primarily in areas lacking evidence of former glaciation, thus aiming at quantifying surface erosion rates. For exposure age data, see Supplementary Dataset.

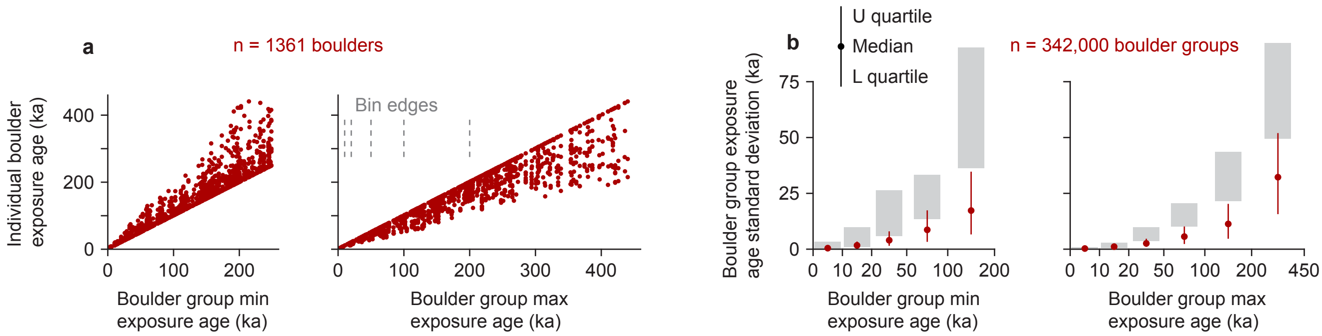

Fig. S8. Simulated exposure ages for the prior exposure model adopting a maximum duration of prior exposure increasing linearly with deglaciation age, from 0 ka (at deglaciation age 0 ka) to 400 ka (at deglaciation age 250 ka), and a maximum prior sample depth of 2 m. (a) Simulated individual exposure ages. (b) Simulated boulder group exposure age spread shown as group standard deviation (median and interquartile range) for bins with bin edges at 10, 20, 50, 100, and 200 ka. The grey areas show the interquartile range of the measured data for comparison. Even with the maximum duration of prior exposure and maximum prior sample depth set to favourable values for high inheritance, the simulated exposure ages have lower age spread than the measured data.

References

Balco, G., Stone, J.O., Lifton, N.A., Dunai, T.J., 2008. A complete and easily accessible means of calculating surface exposure ages or erosion rates from ^{10}Be and ^{26}Al measurements. Quat. Geochron. 3, 174-195.

Chmeleff, J., von Blanckenburg, F., Kossert, K., Jakob, D., 2010. Determination of the ^{10}Be half-life by multicollector ICP-MS and liquid scintillation counting. Nucl. Instrum. Methods. Phys. Res. B 268, 192-199.

Dyke, A.S., Moore, A., Robinson, L., 2003. Deglaciation of North America. Geol. Surv. Canada Open File 1574.

Gosse, J.C., Phillips, F.M., 2001. Terrestrial in situ cosmogenic nuclides: theory and application. Quat. Sci. Rev. 20, 1475-1560.

Granger, D.E., Smith, A.L., 2000. Dating buried sediments using radioactive decay and muogenic production of ^{26}Al and ^{10}Be. Nucl. Instrum. Methods. Phys. Res. B 172, 822-826.

Gyllencreutz, R., Mangerud, J., Svendsen, J.-I., Lohne, Ø., 2007a. A new reconstruction and database of build-up and deglaciation of the Eurasian ice sheet. Bjerknes Days Poster, Bjerknes Centre for Climate Research, Bergen.

Gyllencreutz, R., Mangerud, J., Svendsen, J.-I., Lohne, Ø., 2007b. DATED – a GIS-based reconstruction and dating database of the Eurasian deglaciation. Geol. Surv. Finland Spec. Paper 46, 113-120.

Kleman, J., Jansson, K.N., De Angelis, H., Stroeven, A.P., Hättestrand, C., Alm, G., Glasser, N.F., 2010. North American Ice Sheet build-up during the last glacial cycle, 115-21 kyr. Quat. Sci. Rev. 29, 2036-2051.

Kong, P., Na, C.G., Fink, D., Ding, L., Huang, F.X., 2007. Erosion in northwest Tibet from in-situ-produced cosmogenic ^{10}Be and ^{26}Al in bedrock. Earth Surf. Proc. Land. 32, 116-125.

Korschinek, G., Bergmaier, A., Faestermann, T, Gerstmann, U.C., Knie, K., Rugel, G., Wallner, A., Dillmann, I., Dollinger, G., von Gostomski, C.L., Kossert, K., Maiti, M., Poutivtsev, M., Remmert, A., 2010. A new value for the half-life of ^{10}Be by heavy-ion elastic recoil detection and liquid scintillation counting. Nucl. Instrum. Methods. Phys. Res. B 268, 187-191.

Lal, D., 1991. Cosmic ray labeling of erosion surfaces: in situ nuclide production rates and erosion models. Earth Planet. Sci. Lett. 104, 424-439.

Lal, D., Harris, N.B.W., Sharma, K.K., Gu, Z.Y., Ding, L., Liu, T.S., Dong, W.Q., Caffee, M.W., Jull, A.J.T., 2003. Erosion history of the Tibetan Plateau since the last interglacial: constraints from the ¢rst studies of cosmogenic ^{10}Be from Tibetan bedrock. Earth Planet. Sci. Lett. 217, 33-42.

Owen, L.A., Caffee, M.W., Finkel, R.C., Seong, Y.B., 2008. Quaternary glaciation of the Himalayan-Tibetan orogen. J. Quat. Sci. 23, 513-531.